Study on cosmogenic activation above ground for the DarkSide-20k project

E. Aaron[a], P. Agnes[b], I. Ahmad[c], S. Albergo[d,e], I. F. M. Albuquerque[f],
T. Alexander[g], A. K. Alton[h], P. Amaudruz[i], M. Atzori Corona[j], M. Ave[f],
I. Ch. Avetisov[k], O. Azzolini[l], H. O. Back[g], Z. Balmforth[m],
A. Barrado-Olmedo[n], P. Barrillon[o], A. Basco[p], G. Batignani[q,r], V. Bocci[s],
W. M. Bonivento[j], B. Bottino[t,u,v], M. G. Boulay[w], J. Busto[o], M. Cadeddu[j],
A. Caminata[u], N. Canci[p], A. Capra[i], S. Caprioli[t,u], M. Caravati[j],
N. Cargioli[x,j], M. Carlini[y], P. Castello[z,j], P. Cavalcante[y], S. Cavuoti[aa,p],
S. Cebrian[ab], J. M. Cela Ruiz[n], S. Chashin[ac], A. Chepurnov[ac],
E. Chyhyrynets[l], L. Cifarelli[ad,ae], D. Cintas[ab], M. Citterio[af],
B. Cleveland[ag,ah], V. Cocco[j], E. Conde Vilda[n], L. Consiglio[y], S. Copello[u,t],
G. Covone[aa,p], M. Czubak[ai], M. D'Aniello[aj,p], S. D'Auria[af],
M. D. Da Rocha Rolo[ak], S. Davini[u], S. De Cecco[s,al], D. De Gruttola[am,an],
S. De Pasquale[am,an], G. De Rosa[aa,p], G. Dellacasa[ak], A. V. Derbin[ao],
A. Devoto[x,j], F. Di Capua[aa,p], L. Di Noto[t,u], P. Di Stefano[ap], G. Dolganov[aq],
F. Dordei[j], E. Ellingwood[ap], T. Erjavec[a], M. Fernandez Diaz[n],
G. Fiorillo[aa,p], P. Franchini[ar,m], D. Franco[as], N. Funicello[am,an], F. Gabriele[j],
D. Gahan[x,j], C. Galbiati[v,y,b], G. Gallina[v], G. Gallus[j], M. Garbini[at,ae,ad],
P. Garcia Abia[n], A. Gendotti[au], C. Ghiano[y], C. Giganti[av],
G. K. Giovanetti[aw], V. Goicoechea Casanueva[ax], A. Gola[ay,az], G. Grauso[p],
G. Grilli di Cortona[s], A. Grobov[aq,ba], M. Gromov[ac,bb], M. Guan[bc],
M. Guerzoni[ae], M. Gulino[bd,be], C. Guo[bc], B. R. Hackett[g], A. L. Hallin[bf],
A. Hamer[bg,m], M. Haranczyk[ai], T. Hessel[as], S. Hill[m], S. Horikawa[bh,y],
F. Hubaut[o], J. Hucker[ap], T. Hugues[c], An. Ianni[v,y], V. Ippolito[s],
C. Jillings[ag,ah], S. Jois[m], P. Kachru[b,y], A. A. Kemp[ap], C. L. Kendziora[bi],
M. Kimura[c], I. Kochanek[y], K. Kondo[bh,y], G. Korga[m], S. Koulosousas[m],
A. Kubankin[bj], M. Kuss[q], M. Kuzniak[c], M. La Commara[bk,p], M. Lai[x,j],
E. Le Guirriec[o], E. Leason[m], A. Leoni[bh,y], L. Lidey[g], M. Lissia[j], L. Luzzi[n],
O. Lychagina[bb], O. Macfadyen[m], I. N. Machulin[aq,ba], S. Manecki[ag,ah],
I. Manthos[bl], L. Mapelli[v], A. Margotti[ae], S. M. Mari[bm,bn], C. Mariani[bo],
J. Maricic[ax], A. Marini[t,u], M. Martínez[ab,bp], C. J. Martoff[bq], G. Matteucci[p],
K. Mavrokoridis[br], A. B. McDonald[ap], A. Messina[s,al], R. Milincic[ax],
A. Mitra[bs], A. Moharana[b,y], J. Monroe[m], E. Moretti[ay,az], M. Morrocchi[q,r],
T. Mróz[ai], V. N. Muratova[ao], C. Muscas[z,j], P. Musico[u], R. Nania[ae],
M. Nessi[y], K. Nikolopoulos[bl], J. Nowak[ar], K. Olchansky[i], A. Oleinik[bj],

V. Oleynikov[bt,bu], P. Organtini[v], A. Ortiz de Solórzano[ab], L. Pagani[a],
M. Pallavicini[t,u], L. Pandola[be], E. Pantic[a], E. Paoloni[q,r], G. Paternoster[ay,az],
P. A. Pegoraro[z,j], K. Pelczar[ai], C. Pellegrino[ae], V. Pesudo[n], S. Piacentini[al,s],
L. Pietrofaccia[y], N. Pino[d,e], A. Pocar[bv], D. M. Poehlmann[a], S. Pordes[bi],
P. Pralavorio[o], D. Price[bw], F. Ragusa[bx,af], Y. Ramachers[bs], M. Razeti[j],
A. L. Renshaw[by], M. Rescigno[s], F. Retiere[i], L. P. Rignanese[ae,ad],
C. Ripoli[an,am], A. Rivetti[ak], A. Roberts[br], C. Roberts[bw], J. Rode[av,as],
G. Rogers[bl], L. Romero[n], M. Rossi[u,t], A. Rubbia[au], M. A. Sabia[s,al],
P. Salomone[s,al], E. Sandford[bw], S. Sanfilippo[be], D. Santone[m], R. Santorelli[n],
C. Savarese[v], E. Scapparone[ae], G. Schillaci[be], F. G. Schuckman II[ap],
G. Scioli[ad,ae], M. Simeone[bz,p], P. Skensved[ap], M. D. Skorokhvatov[aq,ba],
O. Smirnov[bb], T. Smirnova[aq], B. Smith[i], F. Spadoni[g], M. Spangenberg[bs],
R. Stefanizzi[x,j], A. Steri[j], V. Stornelli[bh,y], S. Stracka[q], M. Stringer[ap],
S. Sulis[z,j], A. Sung[v], Y. Suvorov[aa,p,aq], A. M. Szelc[bg], R. Tartaglia[y],
A. Taylor[br], J. Taylor[br], S. Tedesco[ca], G. Testera[u], K. Thieme[ax],
T. N. Thorpe[cb], A. Tonazzo[as], A. Tricomi[d,e], E. V. Unzhakov[ao],
T. Vallivilayil John[b,y], M. Van Uffelen[o], T. Viant[au], S. Viel[w],
R. B. Vogelaar[bo], J. Vossebeld[br], M. Wada[c,x], M. B. Walczak[c], H. Wang[cb],
Y. Wang[bc,cc], S. Westerdale[cd], L. Williams[ce], I. Wingerter-Seez[o],
R. Wojaczynski[c], Ma. M. Wojcik[ai], T. Wright[bo], Y. Xie[bc,cc], C. Yang[bc,cc],
A. Zabihi[c], P. Zakhary[c], A. Zani[af], A. Zichichi[ad,ae], G. Zuzel[ai],
M. P. Zykova[k]

[a]*Department of Physics, University of California, Davis, CA 95616, USA*
[b]*Gran Sasso Science Institute, L'Aquila 67100, Italy*
[c]*AstroCeNT, Nicolaus Copernicus Astronomical Center of the Polish Academy of Sciences, 00-614 Warsaw, Poland*
[d]*INFN Catania, Catania 95121, Italy*
[e]*Università of Catania, Catania 95124, Italy*
[f]*Instituto de Física, Universidade de São Paulo, São Paulo 05508-090, Brazil*
[g]*Pacific Northwest National Laboratory, Richland, WA 99352, USA*
[h]*Physics Department, Augustana University, Sioux Falls, SD 57197, USA*
[i]*TRIUMF, 4004 Wesbrook Mall, Vancouver, BC V6T 2A3, Canada*
[j]*INFN Cagliari, Cagliari 09042, Italy*
[k]*Mendeleev University of Chemical Technology, Moscow 125047, Russia*
[l]*INFN Laboratori Nazionali di Legnaro, Legnaro (Padova) 35020, Italy*
[m]*Department of Physics, Royal Holloway University of London, Egham TW20 0EX, UK*
[n]*CIEMAT, Centro de Investigaciones Energéticas, Medioambientales y Tecnológicas, Madrid 28040, Spain*
[o]*Centre de Physique des Particules de Marseille, Aix Marseille Univ, CNRS/IN2P3, CPPM, Marseille, France*

[p] INFN Napoli, Napoli 80126, Italy

[q] INFN Pisa, Pisa 56127, Italy

[r] Physics Department, Università degli Studi di Pisa, Pisa 56127, Italy

[s] INFN Sezione di Roma, Roma 00185, Italy

[t] Physics Department, Università degli Studi di Genova, Genova 16146, Italy

[u] INFN Genova, Genova 16146, Italy

[v] Physics Department, Princeton University, Princeton, NJ 08544, USA

[w] Department of Physics, Carleton University, Ottawa, ON K1S 5B6, Canada

[x] Physics Department, Università degli Studi di Cagliari, Cagliari 09042, Italy

[y] INFN Laboratori Nazionali del Gran Sasso, Assergi (AQ) 67100, Italy

[z] Department of Electrical and Electronic Engineering, Università degli Studi di Cagliari, Cagliari 09123, Italy

[aa] Physics Department, Università degli Studi "Federico II" di Napoli, Napoli 80126, Italy

[ab] Centro de Astropartículas y Física de Altas Energías, Universidad de Zaragoza, Zaragoza 50009, Spain

[ac] Skobeltsyn Institute of Nuclear Physics, Lomonosov Moscow State University, Moscow 119234, Russia

[ad] Department of Physics and Astronomy, Università degli Studi di Bologna, Bologna 40126, Italy

[ae] INFN Bologna, Bologna 40126, Italy

[af] INFN Milano, Milano 20133, Italy

[ag] SNOLAB, Lively, ON P3Y 1N2, Canada

[ah] Department of Physics and Astronomy, Laurentian University, Sudbury, ON P3E 2C6, Canada

[ai] M. Smoluchowski Institute of Physics, Jagiellonian University, 30-348 Krakow, Poland

[aj] Department of Strutture per l'Ingegneria e l'Architettura, Università degli Studi "Federico II" di Napoli, Napoli 80131, Italy

[ak] INFN Torino, Torino 10125, Italy

[al] Physics Department, Sapienza Università di Roma, Roma 00185, Italy

[am] Physics Department, Università degli Studi di Salerno, Salerno 84084, Italy

[an] INFN Salerno, Salerno 84084, Italy

[ao] Saint Petersburg Nuclear Physics Institute, Gatchina 188350, Russia

[ap] Department of Physics, Engineering Physics and Astronomy, Queen's University, Kingston, ON K7L 3N6, Canada

[aq] National Research Centre Kurchatov Institute, Moscow 123182, Russia

[ar] Physics Department, Lancaster University, Lancaster LA1 4YB, UK

[as] APC, Université de Paris, CNRS, Astroparticule et Cosmologie, Paris F-75013, France

[at] Museo Storico della Fisica e Centro Studi e Ricerche Enrico Fermi, Roma 00184, Italy

[au] Institute for Particle Physics, ETH Zürich, Zürich 8093, Switzerland

[av] LPNHE, CNRS/IN2P3, Sorbonne Université, Université Paris Diderot, Paris 75252, France

[aw] Williams College, Physics Department, Williamstown, MA 01267 USA

[ax] Department of Physics and Astronomy, University of Hawai'i, Honolulu, HI 96822, USA

[ay] Fondazione Bruno Kessler, Povo 38123, Italy

3

[az]Trento Institute for Fundamental Physics and Applications, Povo 38123, Italy

[ba]National Research Nuclear University MEPhI, Moscow 115409, Russia

[bb]Joint Institute for Nuclear Research, Dubna 141980, Russia

[bc]Institute of High Energy Physics, Beijing 100049, China

[bd]Engineering and Architecture Faculty, Università di Enna Kore, Enna 94100, Italy

[be]INFN Laboratori Nazionali del Sud, Catania 95123, Italy

[bf]Department of Physics, University of Alberta, Edmonton, AB T6G 2R3, Canada

[bg]School of Physics and Astronomy, University of Edinburgh, Edinburgh EH9 3FD, UK

[bh]Università degli Studi dell'Aquila, L'Aquila 67100, Italy

[bi]Fermi National Accelerator Laboratory, Batavia, IL 60510, USA

[bj]Radiation Physics Laboratory, Belgorod National Research University, Belgorod 308007, Russia

[bk]Pharmacy Department, Università degli Studi "Federico II" di Napoli, Napoli 80131, Italy

[bl]School of Physics and Astronomy, University of Birmingham, Edgbaston, B15 2TT, Birmingham, UK

[bm]INFN Roma Tre, Roma 00146, Italy

[bn]Mathematics and Physics Department, Università degli Studi Roma Tre, Roma 00146, Italy

[bo]Virginia Tech, Blacksburg, VA 24061, USA

[bp]Fundación ARAID, Universidad de Zaragoza, Zaragoza 50009, Spain

[bq]Physics Department, Temple University, Philadelphia, PA 19122, USA

[br]Department of Physics, University of Liverpool, The Oliver Lodge Laboratory, Liverpool L69 7ZE, UK

[bs]University of Warwick, Department of Physics, Coventry CV47AL, UK

[bt]Budker Institute of Nuclear Physics, Novosibirsk 630090, Russia

[bu]Novosibirsk State University, Novosibirsk 630090, Russia

[bv]Amherst Center for Fundamental Interactions and Physics Department, University of Massachusetts, Amherst, MA 01003, USA

[bw]Department of Physics and Astronomy, The University of Manchester, Manchester M13 9PL, UK

[bx]Physics Department, Università degli Studi di Milano, Milano 20133, Italy

[by]Department of Physics, University of Houston, Houston, TX 77204, USA

[bz]Chemical, Materials, and Industrial Production Engineering Department, Università degli Studi "Federico II" di Napoli, Napoli 80126, Italy

[ca]Department of Electronics and Communications, Politecnico di Torino, Torino 10129, Italy

[cb]Physics and Astronomy Department, University of California, Los Angeles, CA 90095, USA

[cc]University of Chinese Academy of Sciences, Beijing 100049, China

[cd]Department of Physics and Astronomy, University of California, Riverside, CA 92507, USA

[ce]Department of Physics and Engineering, Fort Lewis College, Durango, CO 81301, USA

Abstract

The activation of materials due to the exposure to cosmic rays may become an important background source for experiments investigating rare event phenomena. DarkSide-20k is a direct detection experiment for galactic dark matter particles, using a two-phase liquid argon time projection chamber filled with 49.7 tonnes (active mass) of Underground Argon (UAr) depleted in ^{39}Ar. Here, the cosmogenic activity of relevant long-lived radioisotopes induced in the argon and other massive components of the set-up has been estimated; production of 120 t of radiopure UAr is foreseen. The expected exposure above ground and production rates, either measured or calculated, have been considered. From the simulated counting rates in the detector due to cosmogenic isotopes, it is concluded that activation in copper and stainless steel is not problematic. Activation of titanium, considered in early designs but not used in the final design, is discussed. The activity of ^{39}Ar induced during extraction, purification and transport on surface, in baseline conditions, is evaluated to be 2.8% of the activity measured in UAr from the same source, and thus considered acceptable. Other products in the UAr such as ^{37}Ar and ^{3}H are shown to not be relevant due to short half-life and assumed purification methods.

Keywords: Cosmogenic activation, Argon, Dark matter, Rare events

1. Introduction

Great efforts have been devoted worldwide to unravel the nature of the dark matter [1] which could be pervading the galactic halo. One of the strategies followed is the search for Weakly Interacting Massive Particles (WIMPs) by direct detection via WIMP-nucleus elastic scattering. This required making use of different kinds of very sensitive radiation detectors [2, 3]. Noble elements like xenon and argon, being excellent scintillators and easily ionized, are ideal targets and massive experiments based on this detection technique presently have a leading role [4–10].

The expected counting rates from the interaction of WIMPs are extremely low; therefore, dark matter detectors require ultra-low background conditions. Operating in deep underground locations, using active and passive shielding, carefully selecting radiopure materials, and developing background-

rejection methods in analysis are necessary for rare events experiments [11, 12]. In this context, long-lived radioactive isotopes induced in the materials of the experiment by the exposure to cosmic rays at the earth's surface (during fabrication, transport and storage) can be as relevant as residual contamination from primordial nuclides, and they may be very problematic, depending on the target. In principle, cosmogenic activation can be kept under control by minimizing exposure at surface and storing materials underground, avoiding flights, and even using shielding against the hadronic component of cosmic rays. But since these requirements usually complicate the preparation of experiments, it would be desirable to have reliable estimates of activation yields to assess the real danger of exposing materials to cosmic rays. Direct assay measurements of exposed materials, in very low background conditions, and calculations of production rates and yields, following different approaches, have been made for several materials in the context of dark matter, 2β decay, and neutrino experiments [13, 14]. Results have been derived in the last years for detector media like germanium [15–23], silicon [24], NaI [20, 25–28], tellurium and TeO_2 [29–31], xenon [32–34], argon [20, 35, 36] and molybdate [37] as well as for materials commonly used in the set-ups like copper [18, 32, 33, 38, 39], lead [40] or stainless steel [33, 38].

Liquid Argon (LAr) offers important advantages for radiation detection, like a high scintillation yield and easy purification from non-noble contaminants. Radioactive backgrounds that produce electron recoils (ER) can be discriminated from nuclear recoil (NR) events, typically expected from WIMPs, as there is significant difference between the time distribution of their scintillation signals; this provides an outstanding Pulse Shape Discrimination (PSD) power, as shown by the single-phase LAr detector DEAP-3600 with a rejection factor over 10^8 [7]. Dual-phase Time Projection Chambers (TPCs) in which both the primary scintillation and the electroluminescence from electrons are detected have additional capabilities like better position resolution; this was the approach of the DarkSide-50 experiment carried out at the Laboratori Nazionali del Gran Sasso (LNGS) in Italy [8]. DarkSide-50 used Underground Argon (UAr), depleted of ^{39}Ar by a factor 1400±200 with respect to the Atmospheric Argon (AAr) activity of ∼1 Bq/kg. DarkSide-50 demonstrated the dual-phase method also allows for a sensitive search for lighter WIMPs [9, 10] using the electroluminescence signal alone to obtain a lower energy threshold.

Despite these excellent background discrimination capabilities, acceptance losses via ER + NR pile-up in the TPC or accidental coincidence

between signals from the TPC and a veto detector that mimic the neutron capture signature can be produced by γ or β emitters in the set-up and therefore these background sources must be carefully considered too. The goal of this work is to quantify in particular the effect of cosmogenic activation of detector materials on the expected counting rates of the DarkSide-20k detector, considering exposure on the Earth's surface under realistic conditions. This allows requirements and procedures during the preparation and commissioning of the experiment to be set. The study has been carried out for the UAr acting as detector medium as well as for copper, and stainless steel, since the use of large quantities of these materials was foreseen in different components, according to the design of DarkSide-20k. The paper is structured as follows: the DarkSide-20k project is presented in Sec. 2; the methodology applied to quantify cosmogenic activities is described in Sec. 3, showing the obtained results for different materials in Secs. 4, 5 and 6; the counting rates expected from these activities are discussed in Sec. 7, before summarizing conclusions in Sec. 8.

2. The GADMC and the DarkSide-20k detector

Following the success of several LAr dark matter experiments, the Global Argon Dark Matter Collaboration (GADMC) has been established to operate detectors pushing the sensitivity for WIMP detection down to the neutrino floor [41, 42]. As a first step, the DarkSide-20k experiment will be operated in the Hall C of LNGS with ∼20 t of UAr in the fiducial volume; the data taking is intended to start in 2026. The ARGO detector, increasing this volume to ∼360 t, is foreseen towards the end of this decade with a target exposure of several thousand t·y at SNOLAB. ARGO would also have excellent sensitivity to CNO neutrinos and galactic supernovae [43].

2.1. GADMC

One of the goals of GADMC is the procurement of large amounts of low-radioactivity UAr as detector target, which is essential to achieve the scientific goals as the content of ^{39}Ar in AAr would be intolerable; three projects are in development to ensure this:

- Extraction of argon with a naturally low concentration of radioactive ^{39}Ar from an underground source (CO_2 wells) will be carried out at the Urania plant, in Cortez, CO (US). This is the same source of UAr used for the DarkSide-50 detector.

7

- UAr will be further chemically purified to detector-grade argon in the Aria facility, in Sardinia (Itay); Aria will have a 350 m cryogenic distillation column, called Seruci-I, currently being commissioned [44].

- Assessing the ultra-low ^{39}Ar content of the UAr is crucial for the GADMC projects. This is the goal of the DArT detector [45], using a small chamber placed at the centre of the ArDM detector in the Canfranc Underground Laboratory (LSC) in Spain. It aims to measure ^{39}Ar below the mBq/kg level with 10% precision in one week of run.

There is a growing interest in the use of ultra-pure UAr also outside GADMC, as it has potential broader applications for measuring coherent neutrino scattering, environmental assay, neutrinoless 2β decay, and large DUNE-like detectors [46]; the challenges for its production and characterization are carefully addressed in Refs. [47, 48].

2.2. DarkSide-20k

In DarkSide-20k the core of the apparatus is a dual-phase TPC, serving both as WIMP target and detector, filled and surrounded by low-radioactivity UAr; a total of 99.2 t of UAr is required, 51.1 t inside the TPC. The TPC has three dimensional space reconstruction capability that permits the definition of a wall-less fiducial volume. SiPMs read the prompt scintillation in the liquid (S1) and delayed electroluminescence in the gas phase (S2). The TPC is contained in a gadolinium-loaded acrylic vessel (Gd-PMMA), which moderates and captures neutrons after they scatter in the TPC and produce a WIMP-like signal; γ-rays produced by the neutron capturing are detected in the UAr veto surrounding the Gd-PMMA vessel. The TPC is shaped as prism with octagonal base with a vertical drift length of 348 cm and an octagonal inscribed circle diameter of 350 cm. The anode and cathode plates are realized by pure acrylic, PMMA. A total of 8448 and 1920 Photo-Detector Modules (PDMs) view the TPC volume and the inner veto, respectively. The inner veto is housed within a vessel, made of stainless steel, immersed in a bath of 700 t of AAr acting as shield and outer veto detector for muons and associated products. The AAr is contained in a ProtoDUNE-like membrane cryostat. All the materials used to build the whole detector system are carefully selected for low levels of radioactivity. Figure 1 shows cross views of the cryostat and the inner detector. A large amount of Gd-loaded PMMA, of the order of 11 t, is foreseen, but no hint of cosmogenic isotopes has been found
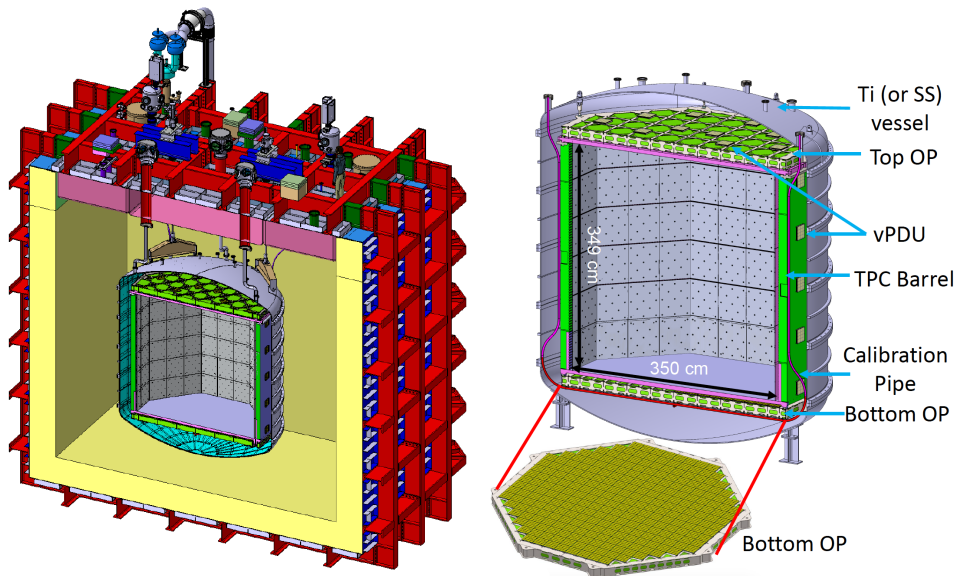
Figure 1: Cross sections of the cryostat of the outer veto (left) and of the vessel containing the inner veto and TPC (right) of the DarkSide-20k detector. OP stands for Optical Plane and PDU for Photo Detection Unit.

in the radiopurity measurements by γ spectroscopy performed for acrylic and Gd_2O_3 samples. Thus activation of this material has not been analyzed. Table 1 lists materials, masses and considered cosmogenic isotopes for the main components in the design.

DarkSide-20k is being designed to operate with <0.1 events over a 200 t·y exposure, thanks to the powerful PSD for ER background and the neutron veto capabilities. For a fiducial mass of 20.2 t, the projected sensitivities are 4.6×10^{-48} cm^2 for the 90% C.L. exclusion and 1.5×10^{-47} cm^2 or the 5σ discovery of a 1 TeV/c^2 WIMP. In parallel, a much smaller detector specifically optimized for the investigation of low-mass dark matter, DarkSide-LowMass, is being considered [49]. Combined, DarkSide-20k, DarkSide-LowMass and ARGO will completely cover the spin-independent WIMP hypothesis parameter space down to the irreducible neutrino background for WIMP masses from 1 GeV/c^2 to several hundreds of TeV/c^2. Planck-scale mass dark matter, already investigated by DEAP-3600 [50], would also require large detectors.

The achievement of an extremely low background rate requires thorough background studies. G4DS [51] is a Monte Carlo (MC) simulation frame-

Table 1: Materials and masses of the main components considered in the design of the DarkSide-20k detector shown in Fig. 1. Cosmogenic isotopes considered for each material in this work are also indicated.

Component	Material	Mass	Induced isotopes
Membrane cryostat	Stainless steel	224.6 t	See Table 2
Outer Veto: filling	AAr	700 t	^{37}Ar, ^{39}Ar, ^{3}H
Inner Veto: vessel	Stainless steel	12 t	See Table 2
TPC: barrel	Gd-loaded PMMA	11 t	-
TPC: grids, frame, brackets	Stainless steel	1055 kg	See Table 2
TPC: cables	Copper	117.8 kg	See Table 2
Inner Veto+TPC: filling	UAr	99.2 t	^{37}Ar, ^{39}Ar, ^{3}H
Electronic components	Copper	47.3 kg	See Table 2

work developed for DarkSide based on Geant4 providing accurate simulation of light production, propagation, and detection for background and signal events. It is designed with a modular architecture in order to include a full description of different detectors: DarkSide-50, DarkSide-20k and ARGO. G4DS has been extensively validated on DarkSide-50 data [51], demonstrating the high accuracy required to optimize the geometry and establish the performance of the TPC and the neutron and muon vetoes for DarkSide-20k. For the TPC, it fully reproduces the responses of the detector in S1, S2, and time, the three primary variables on which the discrimination of β/γ background is based. Great efforts have been devoted to the description of the physical properties of materials, especially the optical ones, exploited by G4DS to track each photon. A spatial event generator is implemented for each detector material in order to generate and track particles emitted by radioactive decays and to assess its impact on the DarkSide-20k background. In addition, an (α,n) event generator, based on the TALYS package[1], is implemented to study the impact of the neutron background and the MC chain is completed by the electronics simulation. γ emissions from the full set of detector components have been simulated to estimate the corresponding background rates in the TPC and in the Veto from activities measured in an extensive material screening campaign based on the combination of different radioassay techniques; discrimination techniques based on energy and position of the interactions are implemented to compute the rate in the fiducial

---

[1]http://www.talys.eu

volume. Preliminary estimates of γ background rates point to values around 50 Hz in the TPC and 100 Hz in the Veto, with dominant contribution from PDMs and, to a lesser extent, from Gd-loaded acrylic. The β contribution of ^{39}Ar, considering the total active mass of UAr in the TPC (50 tonnes) and in the inner veto (32 tonnes) and the measured activity value in DarkSide-50, produces 36 Hz in the TPC and 26 Hz in the Veto.

3. Methodology

One of the most relevant processes in the production of radioactive isotopes in materials is the spallation of nuclei by high energy nucleons; other reactions like fragmentation, induced fission or capture can be important for some nuclei too. On Earth's surface, as the proton to neutron ratio in cosmic rays decreases significantly at energies below the GeV scale because of the absorption of charged particles in the atmosphere, activation by neutrons is usually dominant. Cosmogenic production of radionuclides underground can be considered in many cases negligible, as the flux of cosmic nucleons is suppressed by more than four orders of magnitude for depths of a few tens of meter water equivalent (m.w.e.) [11]. Radiogenic neutrons, with fluxes in deep underground facilities orders of magnitude lower than that of cosmic neutrons on surface, have in addition energies (around a few MeV) too low to produce spallation processes. Activation underground can be induced by muons; muon spallation (virtual photon nuclear disintegration) and electromagnetic and nuclear reactions from secondary particles are the relevant processes. As the muon energy spectra and fluxes depend on depth, underground activation can be very different for different sites and may impose a minimum required depth if on-site activation is problematic.

To quantify the effect of material cosmogenic activation in a particular experiment, the first step is to know the production rates, R, of the relevant isotopes induced in the material targets. Then, the produced activity, A, can be estimated according to the exposure history to cosmic rays; for instance, considering just a time of exposure t_{exp} followed by a cooling time (time spent underground once shielded from cosmic rays) t_{cool}, for an isotope with decay constant λ, the activity can be evaluated as:

$$A = R[1 - \exp(-\lambda t_{exp})] \exp(-\lambda t_{cool}). \tag{1}$$

Finally, the counting rate generated in the detector by this activity can be computed using G4DS [51].

11

Some direct measurements of production rates at sea level have been carried out for a few materials from the saturation activity, obtained by sensitive screening of samples exposed in well-controlled conditions or by irradiating samples in high flux particle beams. However, in many cases, production rates must be evaluated from the flux of cosmic rays, ϕ, and the isotope production cross-section, σ, being both ingredients dependent on the particle energy E:

$$R = N_t \int \sigma(E)\phi(E)dE, \qquad (2)$$

with N_t the number of target nuclei. The spread for different calculations of productions rates is usually important, even within a factor 2 (see for instance Tables 5, 7 and 8). In this work, measured production rates have been used whenever available and dedicated calculations have been performed otherwise.

3.1. Cosmic ray flux

An analytic expression for the cosmic neutron spectrum at sea level is presented by Gordon et al in Ref. [52], deduced by fitting data from a set of measurements for energies above 0.4 MeV; with this parameterization, the integral flux from 10 MeV to 10 GeV is $3.6\times10^{-3}\text{cm}^{-2}\text{s}^{-1}$ (for conditions of New York City). In Ref. [53], a similar parametrization is provided as well as correction factors, f, to the flux when considering exposure at different locations, as it depends on the altitude and geomagnetic rigidity. For example, outside LNGS at an altitude of $\sim$1000 m, a correction factor f =2.1 was estimated [18] and should be considered in case of exposure to cosmic rays there. Alternatively, the EXPACS ("EXcel-based Program for calculating Atmospheric Cosmic-ray Spectrum") program[2] could be used to calculate fluxes of nucleons, muons, and other particles for different positions and times in the Earth's atmosphere; in this way, possible temporal variations of the cosmic rays fluxes are taken into account. Although precise EXPACS calculations are being considered, results presented here are based on the parameterization from Ref. [52] and correction factor from Ref. [53].

3.2. Production cross sections

Concerning the production cross sections, both measurements at fixed energies and calculations using different computational codes must be taken

---

[2]EXPACS: https://phits.jaea.go.jp/expacs/.

into account to choose the best description of the excitation functions $\sigma(E)$. The following sources of data have been considered in this work:

- The Experimental Nuclear Reaction Data database (EXFOR, CSISRS in US) [54] provides nuclear reaction data and then measured production cross sections for a particular target, projectile, energy, or reaction whenever available[3].

- The Silberberg and Tsao equations presented in Refs. [55–57] are semiempirical formulae derived from proton-induced reactions for targets with mass number A $\geq$ 3, for products with A $\geq$ 6 and for energies >100 MeV and integrated in different codes: COSMO (FORTRAN program) [58], YIELDX (FORTRAN routine, including the latest updates of the equations) [57] and ACTIVIA (C++ computer package, using also experimental data when available) [59].

- The MC simulation of the interaction between nucleons or other projectiles and nuclei allows also computation of production cross sections. Many different models and codes have been developed and validated considering the relevant processes (the formation and decay of compound nuclei, the intranuclear cascade of nucleon interactions, deexcitation processes like fission, fragmentation, spallation, or breakup) [60]; some of these models have been implemented in general-purpose codes like Geant4 [61] or FLUKA [62]. Evaluated libraries of production cross sections have been elaborated, covering different types of reactions or projectiles and different energies, like TENDL (TALYS-based Evaluated Nuclear Data Library)[4] [63] (based on the TALYS code, for protons and neutrons with energies up to 200 MeV); JENDL (Japanese Evaluated Nuclear Data Library) [64] High Energy File[5] (based on the GNASH code, for protons and neutrons from 20 MeV to 3 GeV) is an extension of the JENDL-4.0/HE library including results up to 200 MeV; HEAD-2009 (High Energy Activation Data) [65] (for protons and neutrons with higher energies, from 150 MeV up to 1 GeV) uses a

---

[3]EXFOR: http://www.nndc.bnl.gov/exfor/exfor.htm, http://www-nds.iaea.org/exfor/exfor.htm.

[4]https://tendl.web.psi.ch/tendl_2019/tendl2019.html

[5]JENDL HE library, https://wwwndc.jaea.go.jp/ftpnd/jendl/jendl40he.html; https://wwwndc.jaea.go.jp/jendl/jendl.html

selection of models and codes (CEM, CASCADE/INPE, MCNP, etc.) dictated by an extensive comparison with EXFOR data.

4. Cosmogenic yields in Copper and Steel

As in many experiments, a significant amount of copper and stainless steel are used in DarkSide detectors; both materials are known to become activated and different specific studies on their activation are available [13, 14]. The effect on DarkSide-20k of cosmogenic activity in the components made of copper and stainless steel is analyzed here.

4.1. Production rates

The production rates of the radionuclides typically induced in these materials have been selected from measured and calculated results available in the literature [13, 14]. Estimates using ACTIVIA, Geant4, and TALYS codes, among others, have been made. Saturation activities have been measured with sensitive germanium detectors in samples of copper [32, 38, 39] and steel [38], exposed for long times to cosmic rays. In particular, in this work, the production rates from dedicated measurements, using 125 kg of copper provided by Norddeutsche Affinerie (now Aurubis) exposed for 270 days at Gran Sasso and Nironit stainless steel exposed for 314 days, have been considered [38]; values are reproduced in Table 2. Among the different products identified in copper, ^{60}Co has the longest half-life and, unfortunately, there is a significant disagreement on the production rates estimated for it [13, 14]; the measured value in Ref. [38] is higher than most of all the other estimates by a factor of up to a few times. No assessment of ^{60}Co production in stainless steel could be made in Ref. [38], as, being this isotope a typical contaminant in steel, its cosmogenic activity is obscured by previous contamination at similar level; then, the rate derived from Geant4 calculations [33] has been used. Following the half-lives of the different cosmogenic isotopes identified in copper and steel (also shown in Table 2), ^{54}Mn, ^{57}Co and ^{60}Co could be in principle the most relevant products.

4.2. Activity

To assess the possible effect of the cosmogenic isotopes in these materials for DarkSide-20k, activity A has been evaluated considering the selected production rates at sea level, $t_{cool} = 0$ and extreme cases of exposure: $t_{exp} = 1$ month, $t_{exp} = 1$ year and $t_{exp} = 10$ years. It is worth noting that as

14

measured production rates have been taken into account, the deduced activation corresponds to all cosmic ray particles. The final expected activity is obtained from the specific activities derived from the production rates (per mass unit) using Eq. 1 and the mass of all the components used in the experimental set-up, which according to the present design of DarkSide-20k are 165.1 kg of copper (mainly from cables and PDMs electronic components) and 225.655 tons of stainless steel (mainly from cryostat components) plus 12 tonnes from the inner detector.

Table 2 summarizes the total induced activity in copper and stainless steel, respectively, for the relevant isotopes evaluated at the end of the different exposure times; contribution from each individual component is proportional to its mass (see Table 1). Following the decay mode of these nuclei, γ emissions of the order of 1 MeV will be generated around the active volume by this cosmogenic activation. In the case of copper, even assuming 10 years of exposure, the total activity is at the level of 0.5 Bq. The deduced activities can be compared with available measurements from radioassays; for the copper from the Luvata company being considered in DarkSide-20k, the measured activities using a HPGe detector in the Canfranc Underground Laboratory are <0.30 mBq/kg of ^{60}Co and <0.35 mBq/kg of ^{54}Mn; then, this upper limit set for ^{60}Co would correspond to the exposure of a few years. For all stainless steel components, some cosmogenic activities can be at the level of a few hundreds of Bq, even for just 1 year of exposure; ^{54}Mn is identified as a potential relevant contributor to background. Comparing with available measurements from screening, the derived cosmogenic activity of ^{60}Co is much lower than for instance the one measured for the DUNE steel in the Canfranc Underground Laboratory, finding (10.8±0.9) mBq/kg of ^{60}Co and (1.4±0.3) mBq/kg ^{54}Mn; the measured activity of ^{54}Mn would correspond to an exposure of ∼1 year.

5. Cosmogenic yields in Titanium

Titanium is not part of the DarkSide-20k design. However, it was considered in previous designs and titanium is of interest in low-background experiments generally, so we include it here. The possible impact of different cosmogenic products has been analyzed and then, the production rate and induced activity at sea level of the most relevant one, ^{46}Sc, have been quantified from available information and new calculations. To our knowledge, no direct measurement of productions rates for activation is available

for titanium. Natural composition has been assumed.

5.1. Relevant isotopes

Titanium activation by cosmic rays, particularly during air transport, was studied within the DarkSide Collaboration using a modified version of the COSMO code; the induced activity was quantified under different exposure and cooling conditions, including one with an exposure at sea level for a long time (10,000 days). In Ref. [33], the cosmogenic activation at sea level of several materials used in rare event search experiments, including titanium, was quantified from Geant4 simulations (for neutrons, protons and muons considering the Shielding physics list) and using the ACTIVIA code. In both works, the yield of different products was evaluated: some of them (including several Sc isotopes) are short-lived with half-lives of a few days at most; others, like ^{40}K and ^{50}V, are very long-lived, so huge exposures comparable to their half-lives would be required to produce a significant activity; among the isotopes with intermediate half-lives, most of them produce emissions which could not escape from titanium to reach the active volume, as they are either pure or almost pure β^- emitters (^{3}H, ^{33}P, ^{35}S, ^{39}Ar, ^{45}Ca) or generate X-rays or low energy (below $\sim$80 keV) γ rays (^{44}Ti, ^{49}V). Therefore, ^{46}Sc has been identified as the main product which could be relevant and the new calculations performed here correspond just to this isotope.

Table 2: Estimates of induced activity in all copper and stainless steel components of DarkSide-20k at the end of the exposure to cosmic rays. For each one of the products, the half-life [66], main γ emissions and corresponding probabilities are indicated together with the production rates R at sea level assumed (from measurements in Ref. [38] except for ^{60}Co in stainless steel, taken from Ref. [33]) and the total activity A for the three exposure times considered (1 month, 1 year and 10 years).

	^{7}Be	^{46}Sc	^{54}Mn	^{59}Fe	^{56}Co	^{57}Co	^{58}Co	^{60}Co
$T_{1/2}$ (d)	53.22	83.79	312.19	44.49	77.24	271.82	70.85	1923.95
γ emissions (keV)	477.6	889.3, 1120.5	834.8	1099.3, 1291.6	846.8, 1238.3	122.1	810.8	1173.2, 1332.5
probability (%)	10.5	99.98, 99.98	99.98	56.5, 43.2	100, 67.6	85.6	99	99.97, 99.99
Copper								
R (atoms/kg/day)		2.18±0.74	8.85±0.86	18.7±4.9	9.5±1.2	74±17	67.9±3.7	86.4±7.8
A (1 m) (mBq)		0.92±0.31	1.09±0.11	13.3±3.5	4.28±0.54	10.4±2.4	33.0±1.8	1.77±0.16
A (1 y) (mBq)		4.0±1.3	9.39±0.91	35.6±9.3	17.5±2.2	86±20	126.1±6.9	20.3±1.8
A (10 y) (mBq)		4.2±1.4	16.9±1.6	35.7±9.4	18.2±2.3	141±32	129.8±7.1	121±11
Stainless Steel								
R (atoms/kg/day)	389±60	19.0±3.5	233±26		20.7±3.5		51.8±7.8	6.27
A (1 m) (Bq)	346±53	11.5±2.1	41.3±4.6		13.4±2.3		36.2±5.5	0.19
A (1 y) (Bq)	1061±164	49.7±9.2	356±40		54.8±9.3		138±21	2.1
A (10 y) (Bq)	1070±165	52.3±9.6	641±71		56.9±9.6		142±21	13

Table 3: Calculations of the production rate at sea level of ^{46}Sc in titanium in this work and from the literature.

Code	R (atoms/kg/day)	
COSMO	289.4	
ACTIVIA	270.1 6	[33]
Geant4	275.5	[33]
Estimated rate in this work	(271±68)	

^{46}Sc is a β^- emitter with a half-life of 83.8 days and a transition energy of 2366.5 keV [66]; two γ rays of 889.3 keV and 1120.5 keV are produced with almost 100% probability each. Its activity has been quantified in titanium samples screened by different experiments: LUX-ZEPLIN analyzed many items (finding values ranging from 0.2 to 23 mBq/kg, being most of them around a few mBq/kg) and exposed in a controlled way a sample for 6 months measuring afterwards an activity of (4.4±0.3) mBq/kg [67, 68]; XENON1T also analyzed titanium of different grades, measuring activities from 1.0 to 2.7 mBq/kg [69]. In addition, the production rate at sea level of ^{46}Sc was computed using Geant4 and ACTIVIA [33] and can also be deduced from COSMO calculations; Table 3 compares the different estimates, which point to quite similar values.

5.2. Production rate

To evaluate the production rate of ^{46}Sc at sea level using Eq. 2 and the cosmic neutron spectrum from Ref. [52], a selected description of the production cross sections over the whole energy range from threshold up to 10 GeV, considering both neutrons and protons, has been defined. For libraries providing individual reaction cross sections, the mechanisms indicated in Table 4 have been considered. Figure 2 shows the full set of data on total production cross sections taken into consideration from different libraries and a dedicated calculation using YIELDX. Below 100 MeV, there are important discrepancies between libraries and experimental data for protons, although this should not be relevant for neutron activation if specific calculations for neutrons are used; the only two available measurements on cross sections by neutrons are in perfect agreement with TENDL-2019 results. Above 100 MeV, there is a good agreement between different calculations and experimental data for protons (except for one quite old series of data); it is worth noting than the similarity between cross sections for neutrons and protons (usually assumed

Table 4: Production mechanisms for ^{46}Sc in natural Ti isotopes by neutrons and protons.

	Neutrons	Protons
^{46}Ti (8.25%)	(n,p)	
^{47}Ti (7.44%)	(n,pn)	(p,2p)
^{48}Ti (73.72%)	(n,p2n)	(p, 2pn) (p,pd)
^{49}Ti (5.41%)	(n,p3n)	(p,2p2n) (p,2d) (p,pt)
^{50}Ti (5.18%)	(n,p4n)	(p,2p3n) (p,2dn) (p,dt) (p,ptn)

in this range of higher energies) is fully confirmed by JENDL-HE, providing independent results for them.

Taking into account all the available data, the following cross sections $\sigma(E)$ have been considered:

- Below 20 MeV, TENDL-2019, the only results that are available.

- From 20 to 200 MeV, production cross sections by neutrons from TENDL-2019, JENDL-4.0 and JENDL-HE libraries.

- From 200 MeV to 1 GeV, results from JENDL-HE for neutrons and HEAD-2009 library together with YIELDX calculations.

- From 1 to 10 GeV, YIELDX results and data from JENDL-HE for neutrons (extrapolating the last available value at 3 GeV as constant for all higher energies).

Figure 3 presents a closer view of the cross sections actually considered in the calculations of the production rate for the low (top) and high (bottom) energy regions.

The estimated contributions to the production rate of ^{46}Sc for each energy range and selected cross sections are summarized in Table 5. To sum the contributions in the whole energy region, the calculations with the lowest and highest rates in each region have been considered to get mean value and uncertainty from the defined interval (from 202.9 to 338.9 atoms/kg/day); in this way, the final result is (271±68) atoms/kg/day, in very good agreement with all the previous estimates (see Table 3).

5.3. Activity

From the estimated production rate of ^{46}Sc by neutrons at sea level, the corresponding saturation activity according to Eq. 1 is (3.14±0.79) mBq/kg.
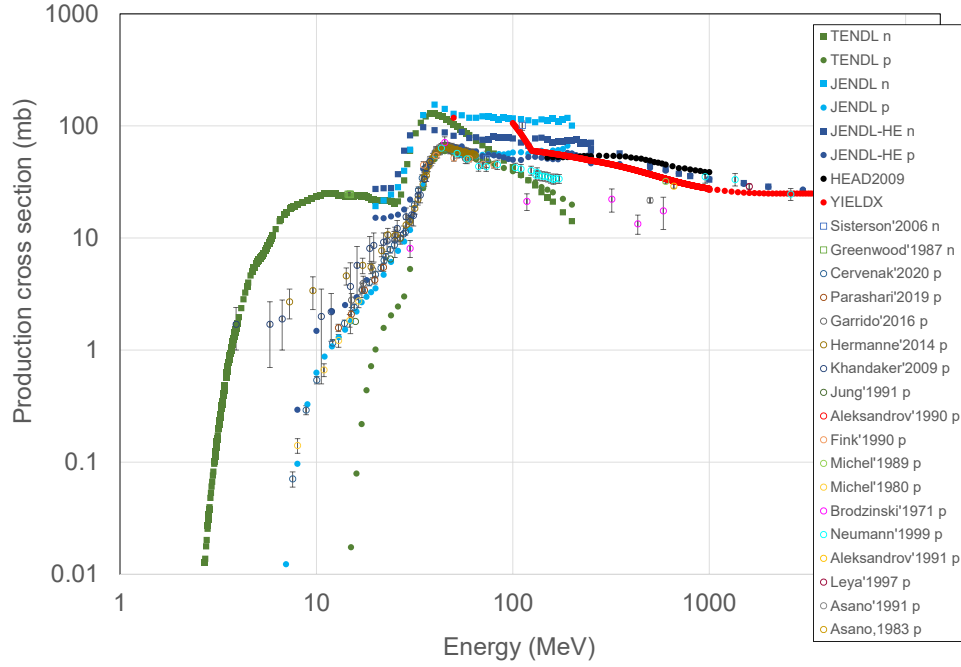
Figure 2: Full compilation of production cross sections of ^{46}Sc in natural Ti by nucleons taken from different sources, including experimental data from the EXFOR database and calculations following different approaches.

Table 5: Contributions to the production rate (in atoms/kg/day) of ^{46}Sc in natural Ti by cosmic neutrons at sea level estimated using Eq. 2, the neutron spectrum from Ref. [52] and the different cross sections selected for each energy range.

	TENDL (n)	JENDL (n)	YIELDX	HEAD2009	JENDL-HE (n)
<20 MeV	16.0				
20-200 MeV	146.6	270.8			187.7
200-1000 MeV			37.9	44.8	49.5
1-10 GeV			2.4		2.6

20
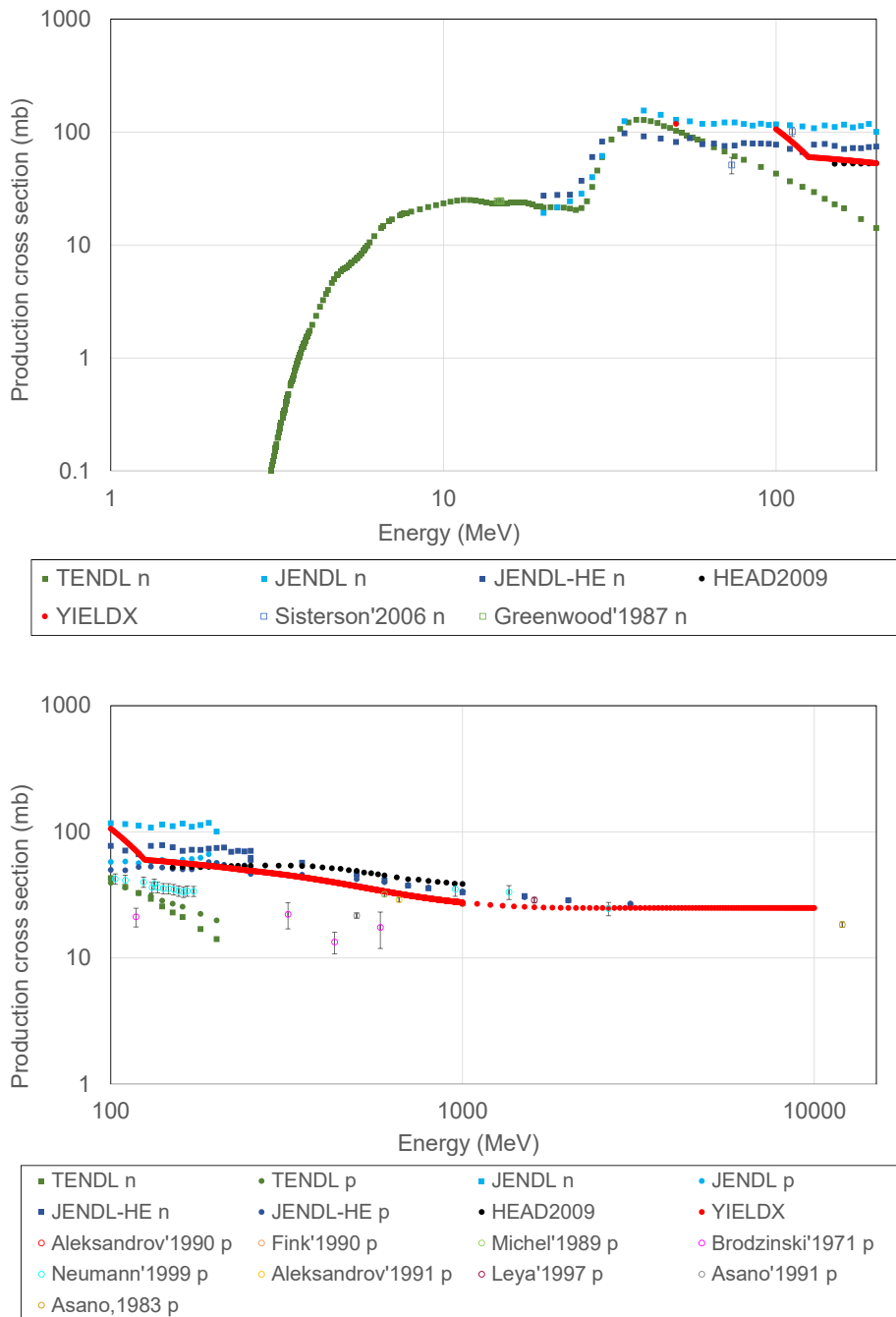
Figure 3: Close view of production cross sections of ^{46}Sc in natural Ti taken into consideration in the estimate of the production rate in the low (top) and high (bottom) energy regions.

21

Due to the half-life of ^{46}Sc, this saturation value may be easily achieved for usual exposure times; indeed, the measured activities of ^{46}Sc in screened samples are around this value. This number can be considered as a conservative assumption for the induced activity at sea level; if exposure happens at certain altitude, correction factors for the cosmic neutron flux should be included. The quantified activity has been obtained just for cosmic neutrons; according to the results based on Geant4 simulations in Ref. [33], the neglected contribution from muons and protons would be just 1.7% of the total. If the vessel of the inner detector was made of titanium, a total mass of 9.5 tons would be used giving an overall activity of around 30 Bq of ^{46}Sc just when finishing the exposure to cosmic rays. According to the current schedule for the installation of the detector, it will be underground more than 1.5 y before starting operation; then, after this cooling period, ^{46}Sc activity would have been reduced to 1.1% of the initial value.

6. Cosmogenic yields in Argon

Argon in the atmosphere contains stable ^{40}Ar at 99.6%; cosmogenically produced radioactive isotopes, mainly ^{39}Ar but also ^{37}Ar or ^{42}Ar, can be a significant background if argon obtained from air is used. The concentration of these three isotopes is much reduced in UAr, but the production of cosmogenic radionuclides after extraction must be taken into consideration.

6.1. Relevant isotopes

^{39}Ar is a β^- emitter with a transition energy of 565 keV and half-life of 269 y [70]; it is mainly produced by the ^{40}Ar(n,2n)^{39}Ar reaction started by cosmic neutrons [35]. The typical activity of ^{39}Ar in AAr is at the level of $\sim$1 Bq/kg, as quantified by WARP [71], ArDM [72] and DEAP [73]. In UAr, after a first study on argon from deep underground sources [74], the measured activity of ^{39}Ar in the DarkSide-50 detector was (0.73 ± 0.11) mBq/kg following a campaign of extracting and purifying argon from deep CO_2 wells in Colorado, US; as mentioned in Sec. 1, this means a reduction of a factor $(1.4\pm0.2)\times10^3$ relative to the AAr [8].

Presence of cosmogenically produced ^{37}Ar was also detected in the beginning of the run of the DarkSide-50 detector with UAr [8]. It decays 100% by electron capture to the ground state of the daughter nuclei with a half-life of 35.02 days [66]; then, the binding energy of electrons from K-shell (2.8 keV, at 90.21%) and L-shell (0.20-0.27 keV, at 8.72%) can be measured

as a distinctive signature. The main production channel is the ^{40}Ar(n,4n)^{37}Ar reaction [35]. Production underground in UAr by thermal and epithermal neutron capture is negligible, as for ^{39}Ar, considering rates as in Ref. [35] and neutron fluxes at LNGS.

^{42}Ar is a pure β^- emitter with a 32.9 y half-life and transition energy of 599 keV, generating ^{42}K, also a β^- emitter with half-life of 12.36 h and transition energy of 3525 keV [70]; this isotope can affect neutrinoless 2β experiments using liquid argon as refrigerant and shielding, as shown by the GERDA experiment [75]. There are two mechanisms for the production of ^{42}Ar in AAr: a two-step neutron capture (requiring a high neutron flux because of the half-life of ^{41}Ar, being of 1.8 h) and the (α,2p) reaction on ^{40}Ar [76]. The specific activity of ^{42}Ar has been studied in the context of different experiments using argon like ICARUS [77], DBA giving 92^{+22}_{-46} μBq/kg [78] and, more recently, DEAP, measuring 40.4 ± 5.9 μBq/kg [73]. The content of ^{42}Ar could not be quantified in DarkSide-50. For UAr, ^{42}Ar should be considered as a potential background for neutrinoless 2β decay searches (for example, by doping LAr with ^{136}Xe); but the threshold for the α reaction on ^{40}Ar is much higher than the energy of α particles from natural radioactivity, according to cross section values from TALYS and other sources [36]. This is also the case for other processes which could produce ^{42}Ar underground from the rock, like ^{43}Ca(n,2p)^{42}Ar or ^{44}Ca(n,n2p)^{42}Ar, when considering the typical energies of radiogenic neutrons from natural fission and (α,n) reactions. The production rate of ^{42}Ar in UAr at sea level from fast neutrons and high energy muons and protons has been evaluated by Geant4 simulation as 5.8×10^{-3} atoms/kg/day in Ref. [36]; this rate would give a saturation activity about three orders of magnitude lower than measured values in AAr. Taking all this into account, the effect of ^{42}Ar in DarkSide-20k will not be considered here although a specific study to quantify radiogenic and cosmogenic production in the Earth's crust is underway[6].

^{3}H in the detector medium of a dark matter experiment can be a very relevant background source due to its decay properties: it is a pure β^- emitter with transition energy of 18.6 keV and a long half-life of 12.3 y [66]. The quantification of its cosmogenic production is not easy, neither by calculations (^{3}H can be generated by different reaction channels) nor experimentally (the β emissions are hard to disentangle from other background contribu-

---

[6]https://indico.sanfordlab.org/event/29/contributions/487/

tions). Estimates of the ^{3}H production rate in several dark matter targets were attempted in Ref. [79]; the rate has been measured for germanium from EDELWEISS [19] and CDMSlite [21] data and for silicon and NaI(Tl) from neutron irradiation [24, 28]. Possible presence of ^{3}H has been observed also in NaI(Tl) crystals by ANAIS [25, 80] and COSINE experiments [27, 81]. In principle, purification systems for LAr may remove all non-noble radionuclides and ^{3}H should not be a problem for DarkSide. This was also assumed for liquid xenon, but ^{3}H was considered as a possible explanation for the excess of electronic recoil events observed in the XENON1T experiment below 7 keV [82, 83], which has disappeared in XENONnT [5]. Activated ^{3}H is separated from argon with SAES Getters [84] and will be removed *in situ* while the UAr recirculates.

Production of other radioisotopes with half-lives longer than 10 days in argon was predicted by using the COSMO code, like ^{7}Be and ^{22}Na (giving γ emissions) and ^{32,33}P and ^{35}S (being pure β^- emitters); production rates at sea level from fast neutrons, high energy muons and protons have been evaluated by Geant4 simulation in Ref. [36]. Assuming an efficient purification of non-noble isotopes, they will not be considered in this study.

6.2. Production rates

The production rates of ^{37}Ar and ^{39}Ar from cosmic neutrons at sea level were measured for the first time through controlled irradiation at Los Alamos Neutron Science Center (LANSCE) with a neutron beam resembling the cosmic neutron spectrum and later direct counting with sensitive proportional counters at Pacific Northwest National Laboratory (PNNL) [35]. Samples of both AAr and UAr were irradiated. In addition, the study of other production mechanisms due to muon capture, cosmic protons and high energy γ rays at the Earth's surface was made using available cross sections to compute total production rates at sea level. The production rates obtained in Ref. [35] for UAr are reproduced in Table 9 as they will be used to evaluate the induced activity in DarkSide-20k. In addition, the production rates of both ^{37}Ar and ^{39}Ar at sea level have been recently evaluated by Geant4 simulation in Ref. [36] too.

The UAr to be used in DarkSide-20k is obtained in Colorado, which is placed at a quite high altitude; then, the corresponding correction factors f to the cosmic ray flux must be taken into consideration. In Ref. [53], high values of f are reported for neutrons at Colorado locations: 4.11 and 12.86 for Denver (at 5280 feet) and Leadville (at 10200 feet), respectively.

24

Table 6: Calculation of the correction factor f to be applied to the cosmic neutron flux at sea level (in New York) for the location of the Urania facilities in Colorado. The relative intensities I are derived from Eq. 3. The final factor for Urania is the average between the deduced ones from Denver and Leadville data.

Location	H (ft)	A (g/cm^2)	f from Ref. [53]	Relative I to Urania	Deduced f for Urania
Denver	5280	852.3	4.11	0.659	6.24
Leadville	10200	705.2	12.86	1.942	6.62
Urania	7100	795.5			6.43

These correction factors f have been adjusted to the altitude at the Urania facilities (at 7100 feet), assuming that the ratio of f for different altitudes is the same than the ratio of cosmic flux intensities. As described in Ref. [53], the intensities I_1 and I_2 at two different altitudes A_1 and A_2 (converted to g/cm^2) are related as:

$$I_2 = I_1 \exp[(A_1 - A_2)/L], \qquad (3)$$

being L the absorption length for the cosmic ray particles. Calculations for the cosmic neutron flux correction factor are summarized in Table 6, using $L = 136$ g/cm^2; the final result for Urania is the average between the deduced ones from Denver and Leadville data, $f = 6.43$. For cosmic protons and muons, the correction factors have been obtained just from Eq. 3 considering the corresponding absorption lengths ($L = 110$ g/cm^2 for protons and $L = 261$ g/cm^2 for muons [53]); the results are $f = 8.67$ for protons and $f = 2.48$ for muons.

Following Eq. 2, a calculation of the production rates of relevant isotopes in argon (assuming 100% ^{40}Ar) by cosmic neutrons from Ref. [52] has been made considering a selection of excitation functions from libraries and YIELDX calculations. Figure 4 shows the available information on production cross sections of ^{3}H, ^{37}Ar and ^{39}Ar by nucleons. For ^{39}Ar, although no experimental data at EXFOR was found for the total production cross section, there are results for partial (n,2nγ) reactions in natural argon at 1-30 MeV taken from Ref. [85]. For ^{3}H, an irradiation experiment with neutrons having an energy spectrum peaked at 22.5 MeV measured the corresponding production cross section [86].

The matching of the cross section data from different libraries, focused on different energy ranges, is not good. Several descriptions of the cross
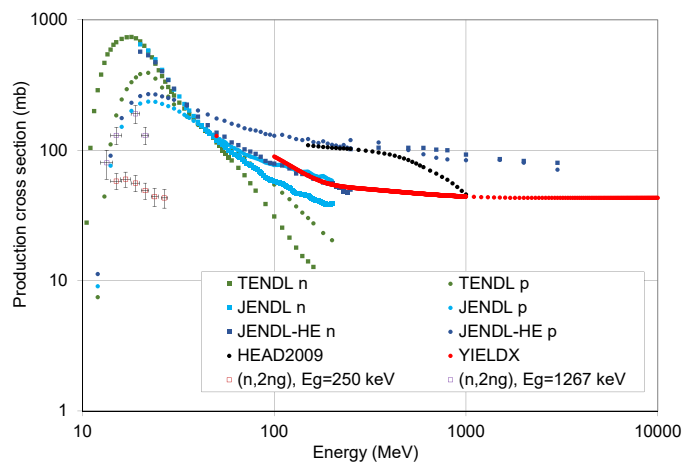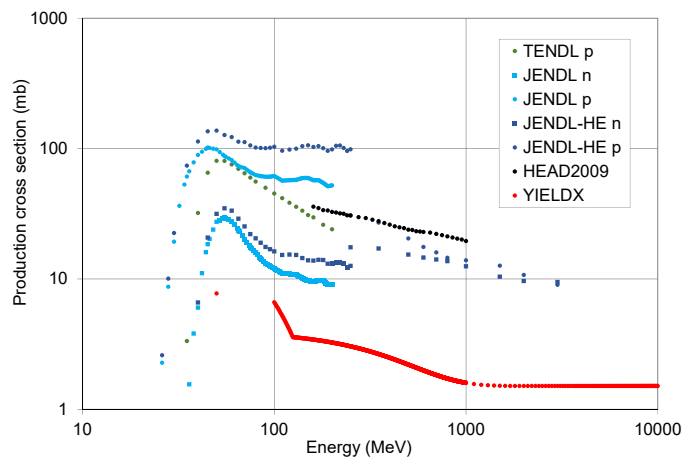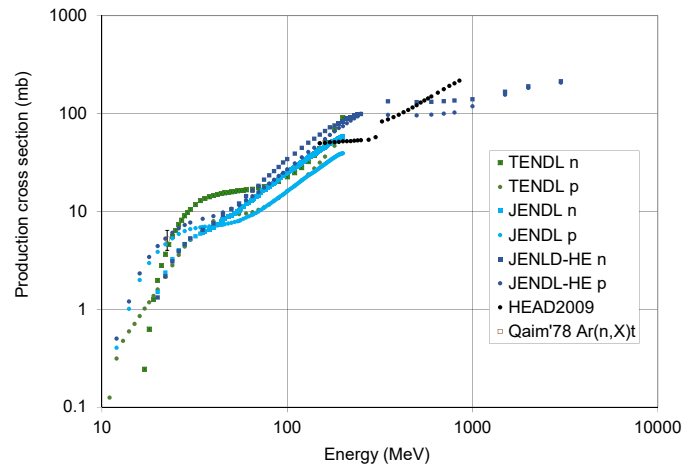
Figure 4: Production cross sections of ^{3}H (top), ^{37}Ar (medium) and ^{39}Ar (bottom) in ^{40}Ar by nucleons taken from different sources.

sections, even from different libraries below and above a particular energy cut, have been considered to estimate the corresponding uncertainty; the obtained maximum and minimum rates define an interval, whose central value and half width have been considered as the final result and its uncertainty for the evaluation of the production rates. Table 7 presents the obtained results for ^{37}Ar and ^{39}Ar, together with the measured production rate for fast neutrons and different calculations from Refs. [35, 36]. The production rate of ^{39}Ar derived here is fully compatible with the measured value (and with several of the calculations in Ref. [35]). The production rate of ^{37}Ar is a factor 2 higher than the measured one, but lower than the Geant4 estimate in Ref. [36]. For calculating final activity yields of ^{37}Ar and ^{39}Ar, the values of the total production rates obtained in Ref. [35] will be used; but this comparison can be useful to assess the reliability of the production rates of isotopes estimated only from calculations, like is the case of ^{3}H in argon.

Evaluations of the production rate of ^{3}H for several targets were applied also for argon, using different codes like TALYS [16] and Geant4 and AC-TIVIA [33]. It was also computed in Ref. [79] for cosmic neutrons, from a selection of excitation functions considering the TENDL and HEAD2009 libraries, following the same approach applied here; this study was cross-checked against experimental data for NaI and germanium, reproducing properly measured production rates [19, 21, 28]. Now, new data for neutron cross sections taken from the JENDL-HE library have been added in the analysis in this work (giving a production rate of 221.6 atoms/kg/day) and then the final production rate has been re-evaluated considering all the other previous estimates in Ref. [79] as (168±53) atoms/kg/day. It must be noted that this value gives only production by neutrons; assuming equal flux and cross sections of protons and neutrons above 1 GeV, it is estimated that protons would increase the rate by 10% at most. Table 8 summarizes all the results for ^{3}H production in argon; an important dispersion of values is found.

Table 7: Calculations of the production rates R of ^{37}Ar and ^{39}Ar in Ar at sea level from this work considering different descriptions of the excitation functions below (LE) and above (HE) a cut energy value; the final estimated rates are given by the ranges defined between the maximum and minimum obtained rates (see text). Different calculations from the literature (considering the same cosmic neutron spectrum from Ref. [52]) and the measured value for fast neutrons from Ref. [35] are also shown for comparison.

		^{37}Ar			^{39}Ar	
This work	Cut	R		This work	Cut	R
LE+HE	(MeV)	(atoms/kg/day)		LE+HE	(MeV)	(atoms/kg/day)
TENDL(p)+HEAD2009	150	153.6		TENDL+HEAD2009	150	726.4
TENDL(p)+YIELDX	100	93.5		TENDL+YIELDX	100	697.1
TENDL(p)+YIELDX	200	122.7		TENDL+YIELDX	200	646.0
JENDL-HE(n)	30	63.9		TENDL+JENDL-HE(n)	20	804.3
Estimated rate in this work		109±45		Estimated rate in this work		725±79
Measurement [35]		51.0±7.4				759±128
ACTIVIA [35]		17.9±2.2				200±25
MENDL-2P [35]		155±19				188±24
TALYS [35]		76.8±9.6				753±94
INCL++ (ABLA07) [35]		79.3±9.9				832±104
				TENDL-2015 [35]		726±91
Geant4 [36]		176				858

Table 8: Production rate R of ^{3}H in Ar at sea level from this work and from different calculations from the literature.

	R (atoms/kg/day)
Estimated rate in this work	168±53
TENDL+HEAD2009 [79]	146± 31
TALYS [16]	44.4
Geant4 [33]	84.9
ACTIVIA [33]	82.9

6.3. Activity

The possible activity yields of relevant cosmogenic isotopes in Ar have been analyzed for the DarkSide-20k detector considering Ar extraction, storage and transportation and taking into account not only cosmogenic neutrons but also other cosmic ray components. For ^{37}Ar and ^{39}Ar, the production rates at sea level precisely determined with the LANSCE neutron beam and the estimates for muons, protons and cosmic γ rays [35] have been considered, while for ^{3}H the production rate estimated in this work has been assumed.

It is planned to produce 120 t of UAr for DarkSide-20k, allocated as follows: 100 t needed for filling the DarkSide-20k TPC, 4 t used during conditioning and purging the cylinder skids, 4 t of argon left in Aria after purification, and 12 t for contingency. The UAr extracted at the Urania plant will be shipped firstly to the Aria facility for purification and then to LNGS for storage and final operation. The current baseline design is to ship the UAr in commercially available high-pressure (517 bar) gas cylinders that are organized into skids capable of containing ∼2 t of UAr each. It is not possible to predict accurately the final exposure conditions for the UAr, but according to the present specifications of Urania and Aria, a baseline exposure history with defined exposure times and places for the different steps of the transportation process can be established and the main sources of uncertainty in the process identified; then, activity yields have been computed for the baseline exposure and the effect of uncertainties assessed. The following steps are foreseen:

1. Storage of UAr at Urania: three skids will be filled before starting transportation. Considering the time required to fill one, exposures of 8, 16 and 24 days have been assumed for each one of the three skids. While at the Urania site, the UAr will always be on the surface while

being processed and once in the skids. The correction factors to the sea level fluxes of cosmic neutrons, protons and muons evaluated for Urania location in Colorado (see Sec. 6.2) have been included in this step.

2. Trip from Urania to a shipping port: a container with the three skids will transport the UAr from Urania to Houston by truck. An exposure of 7 days has been considered. To take into account the different altitude across the trip, the average between the maximal (from Urania altitude) and minimal (at sea level) expected activity has been calculated.

3. Trip overseas to Europe: 60 days of exposure at sea level have been conservatively assumed for the trip by boat from Houston to Cagliari. An additional exposure of 7 days is foreseen for custom issues and the trip from Cagliari to the Aria location.
Steps 1 to 3 will be repeated over twenty times, running in parallel. In total, 16 months are required for completing the extraction and transportation of all the necessary UAr at Urania.

4. Processing and storage of UAr at Aria: once in Sardinia, the skids will be stored near Aria and the UAr will be accumulated for processing. At a purification rate of 1 ton per day, a minimal exposure of 120 t is foreseen. Purified UAr will be stored locally in Sardinia until needed for filling into DarkSide-20k. Underground storage at a depth of at least some tens of m.w.e. would be recommended but, if not possible, a virtually linear increase of 2.6 μBq/kg in the activity of ^{39}Ar should be considered per month of additional exposure at sea level.

5. Trip from Aria to LNGS: 10 days of exposure at sea level have been considered for this trip by boat. It is expected to ship 12 t at a time using six skids; then, this action should be repeated over ten times.

6. Storage at LNGS: skids will be stacked underground as they arrive.

All in all, under these assumptions, the total time from the beginning of production at Urania to the end of processing at Aria is 614 days. If transport from Aria to LNGS starts once all the UAr has been processed, 100 additional days would be required to have all the UAr at LNGS.

Taking into account this exposure history, the induced activity by each cosmic ray component has been computed for each one of the exposure steps (at Urania, trip in US, overseas, at Aria and trip in Italy) from Eq. 1. Tables 9 and 10 show separately each contribution for ^{39}Ar and ^{37}Ar and for ^{3}H,

respectively. The decay of the activities induced at each step during the rest of the whole process is negligible for ^{39}Ar and small for ^{3}H, due to their long half-lives, but extremely relevant for ^{37}Ar; it is accounted for in the final activities reported in Tables 9 and 10.

For both ^{39}Ar and ^{37}Ar, cosmogenic neutrons are responsible of the main part of the induced activity. Under the assumed baseline conditions, the relative contributions to the final ^{39}Ar activity of each exposure step are the following: Urania, 34.4%; US trip, 9.0%; overseas trip, 27.7%; at Aria, 24.8%; and Italy trip, 4.1%. The exposure at Urania gives the largest contribution, followed by that of the overseas trip and at Aria. For ^{37}Ar, having a much shorter half-life, the last exposure during the Italy trip is dominant, producing 55% of the final activity. Concerning ^{3}H, the final activity in Table 10 would apply if no purification procedure was considered; however, if a 100% efficient removal of ^{3}H was achieved in Aria, only the activity in the last step for exposure in Italy would be produced. Table 11 summarizes the expected activities once all the UAr is at LNGS. From values in Table 9, the final estimated activity of ^{39}Ar is (20.7±1.5) μBq/kg; this equals 2.8% of measured activity in DarkSide-50. For ^{37}Ar, the effect of cooling is very important and the expected activity when all the UAr is at LNGS is (103.0±8.6) μBq/kg. From values in Table 10 for ^{3}H, an activity of (2.97±0.94) μBq/kg is expected at that time considering only activation after ideal purification in Aria; with no purification, it would be around 25 times higher.

Uncertainties quoted for activities in Tables 9 and 10 come from those of production rates. Concerning the correction factors of sea level cosmic ray fluxes for exposure at Urania, it has been checked that considering a description different to that applied in Sec. 6.2 produces very similar results; correction factors computed from EXPACS spectra in the energy range relevant for activation (1 MeV to 10 GeV) are $f = 6.09$ for neutrons, $f = 7.60$ for protons and $f = 1.61$ for muons, giving a small decrease in the final activities: 1.0% for ^{39}Ar, no change for ^{37}Ar and 1.5% for ^{3}H with no purification. On the other hand, unexpected events can produce relevant deviations from the baseline exposure conditions and their effect on the activation yields has been assessed. Doubling the exposure at Urania would increase the final ^{39}Ar activity from (20.7±1.5) μBq/kg to (27.7±2.4) μBq/kg, which would be 3.8% of the DarkSide-50 activity. Exposure at Aria has been evaluated for the moment considering just the processing time, but activation produced in the periods before and after the processing should be added if storage is made above ground; to produce an additional 10% of the measured activity in

DarkSide-50 (which was determined with an uncertainty of 14%), 28 months of additional exposure would be required, which is well above the period of 16 months needed for the extraction of the whole amount of UAr needed. All in all, it can be concluded that there is enough contingency in the plan for production, storage and shipping of the UAr so that cosmogenic ^{39}Ar activity does not endanger DarkSide-20k sensitivity.

7. Expected counting rates in DarkSide-20k

As described in Secs. 4.2 and 5.3, ^{54}Mn in stainless steel and ^{46}Sc in titanium are identified as the most relevant cosmogenic products in these materials. The effect of their contribution to the γ background of the experiment has been evaluated finding for the former a negligible contribution in comparison to the other sources of γ background. In a hypothetical detector using a titanium vessel and considering the saturation activity when going underground, ^{46}Sc would add (0.41±0.10) Hz and (21.1±5.3) Hz, respectively, to the estimated counting rates in the TPC and inner veto (see Table 11).

The rates from the estimated cosmogenic activity of products in UAr, under the assumed baseline exposure conditions, are also shown in Table 11. Induced ^{39}Ar due to the whole exposure from Urania to LNGS would add a rate of (1.035±0.075) Hz for the TPC. The contribution of ^{3}H to the TPC counting rate is negligible (around 0.15 Hz) provided an efficient purification at Aria is achieved while that of ^{37}Ar (being (5.15±0.43) Hz if data taking started just immediately after the arrival of all the UAr at LNGS) will decay very quickly. Comparing these numbers with the total β and γ rates presented in Sec. 2.2, it can be concluded that cosmogenic activity does not produce a problematic increase of the TPC and Veto rates.

8. Conclusions

For DarkSide-20k, material cosmogenic activation is a source of β/γ background and it has been quantified for LAr and other massive components from realistic exposure conditions in order to assess the contribution to the counting rates and decide if additional exposure restrictions are necessary. Main results are summarized in Table 11.

Table 9: Calculation of the expected induced activity in kg^{-1} d^{-1} of ^{39}Ar and ^{37}Ar in the UAr of the DarkSide-20k detector, for the assumed production rates R and exposure times (see text). Different columns and rows show separate contributions by cosmic ray components and exposure steps, respectively; relative contributions of each component to the total activity are also quoted. Row labelled as "Final" presents the sum of final activities from all exposure steps including properly their decays.

^{39}Ar	Neutrons	Muons	Protons	γ rays	Total
R (atoms/kg/day) [35]	759±128	172±26	3.6±2.2	112.8±20.9	
Urania	0.551±0.093	0.0483±0.0073	0.0035±0.0022	0.0127±0.0024	0.616±0.093
US	0.139±0.024	0.0148±0.0022	0.0009±0.0005	0.0056±0.0010	0.161±0.024
Overseas	0.359±0.061	0.081±0.012	0.0017±0.0010	0.053±0.010	0.495±0.063
Aria	0.321±0.054	0.073±0.011	0.0015±0.0009	0.048±0.0088	0.444±0.056
Italy	0.0536±0.0090	0.0121±0.0018	0.0003±0.0002	0.0080±0.0015	0.0739±0.0093
Final	1.42±0.13	0.229±0.018	0.0078±0.0026	0.127±0.014	1.79±0.13
(%)	79.6	12.8	0.4	7.1	

^{37}Ar	Neutrons	Thermal neutrons	Protons	γ rays	Total
R (atoms/kg/day) [35]	51±7.4	0.9±0.3	1.3±0.4	3.5±0.7	
Urania	87±13	2.99±0.92	0.93±0.19	0.239±0.080	91±13
US	24.5±3.6	0.81±0.25	0.453±0.091	0.116±0.039	25.9±3.6
Overseas	37.5±5.4	0.95±0.29	2.57±0.51	0.66±0.22	41.7±5.5
Aria	35.5±5.1	0.90±0.28	2.43±0.49	0.63±0.21	39.4±5.2
Italy	9.2±1.3	0.234±0.072	0.63±0.13	0.162±0.054	10.2±1.3
Final	8.03±0.74	0.209±0.040	0.524±0.070	0.135±0.030	8.90±0.75
(%)	90.3	2.3	5.9	1.5	

Table 10: Calculation of the expected induced activity in kg^{-1} d^{-1} of ^3H by cosmic neutrons in the UAr of the DarkSide-20k detector, for the production rate R estimated in this work and the assumed exposure times (see text), considering no purification procedure. Different rows show separate contributions by exposure steps. Row labelled as "Final" presents the sum of final activities from all exposure steps including properly their decays

$^3\mathbf{H}$	Neutrons
R (atoms/kg/day)	168±53
Urania	2.66±0.84
US	0.67±0.21
Overseas	1.73±0.54
Aria	1.55±0.49
Italy	0.259±0.082
Final	6.5±1.1

Table 11: Summary table of estimated activation in DarkSide-20k including isotope, material, main production channel, calculation details, overall activity and counting rates in TPC and inner veto. All reported activity and rate values correspond to the moment when the materials are brought underground. For ^{3}H, row (1) and (2) assume no purification and ideal purification at Aria, respectively.

Isotope	Material	Main channel	Calculation	Activity (μBq/kg)	TPC rate (Hz)	Veto rate (Hz)
^{39}Ar	UAr	^{40}Ar(n,2n)^{39}Ar	Production rates from [35]	20.7±1.5	1.035±0.075	0.662±0.048
^{37}Ar	UAr	^{40}Ar(n,4n)^{37}Ar	Production rates from [35]	103.0±8.6	5.15±0.43	3.30±0.28
^{3}H (1)	UAr	^{40}Ar(n,*)^{3}H	σ(E) in Fig. 4+Gordon spectrum	76±12	3.80±0.60	2.43±0.38
^{3}H (2)	UAr	^{40}Ar(n,*)^{3}H	σ(E) in Fig. 4+Gordon spectrum	2.97±0.94	0.148±0.047	0.095±0.030

For copper and stainless steel components, activation yields of isotopes with relevant half-lives (like ^{54}Mn, ^{57}Co and ^{60}Co) have been computed from measured production rates at sea level at Ref. [38]. In copper, even for 10 y of exposure to cosmic rays, estimated activities are below 0.5 Bq. In stainless steel, hundreds of Bq are expected for some isotopes for just 1 y exposure; the contribution to the counting rate of ER-like events in the TPC from ^{54}Mn activity induced in steel components has been found to be negligible in comparison to the estimated total rate from β/γ backgrounds. This allows to relax additional limitations on the surface residency time.

For natural titanium, ^{46}Sc has been identified as the main cosmogenic product. Other radioisotopes induced are not considered as a potential relevant background due to their half-lives or because their short-range emissions are not expected to escape from titanium. The production rate at sea level of ^{46}Sc has been calculated from a selection of production cross sections and considering the Gordon et al parametrization [52] for the cosmic neutron spectrum, deriving a value of (271$\pm$68) atoms/kg/day, which is in very good agreement with totally different estimates based on modified COSMO, Geant4 simulation and the ACTIVIA code. The corresponding saturation activity is (3.14$\pm$0.79) mBq/kg, in the range of most of the measurements of ^{46}Sc activity in samples found in the literature. Assuming exposure at sea level for a long time, this saturation activity has been conservatively considered to quantify by MC simulation the possible effect of ^{46}Sc emissions on the ER background rate of DarkSide-20k if titanium was used, showing a contribution to the TPC counting rate which is non-relevant, specially when taking into account the cooling down underground before the start of the data taking.

A total of 120 t of UAr depleted in ^{39}Ar must be extracted and processed for filling the TPC and inner veto of DarkSide-20k. The possible induced activity on surface, from the extraction at Urania to the storage at LNGS, has been analyzed not only for ^{39}Ar but also for ^{37}Ar and ^{3}H. Production rates from Ref. [35], based on a neutron irradiation experiment, have been considered for the Ar isotopes while for ^{3}H an estimate of the production rate by cosmic neutrons made in this work obtaining (168$\pm$53) atoms/kg/day has been used. The estimated cosmogenic activity of ^{39}Ar when all the UAr arrives to LNGS, (20.7$\pm$1.5) μBq/kg for the assumed baseline exposure history, is considered acceptable as it is just 2.8% of the residual activity measured in DarkSide-50 for UAr of the same source and would add $\sim$1 Hz to the counting rate of the TPC. The quantified effect of some uncertain steps in

the procedure of UAr production shows that there is enough contingency. Contributions from the induced activity of ^{37}Ar and ^{3}H are not problematic thanks to short half-life and purification, respectively. The results of this study of the cosmogenic activation of UAr will be useful to set exposure limitations for the procurement of the large amounts of radiopure UAr necessary in future LAr projects.

Acknowledgements

References

[1] G. Bertone and D. Hooper, History of dark matter, Rev. Mod. Phys. 90 (2018) 045002, https://doi.org/10.1103/RevModPhys.90.045002.

[2] M. Schumann, Direct Detection of WIMP Dark Matter: Concepts and Status, J. Phys. G: Nucl. Part. Phys. 46 (2019) 103003, https://doi.org/10.1088/1361-6471/ab2ea5.

[3] J. Billard et al, Direct Detection of Dark Matter – APPEC Committee Report, Rep. Prog. Phys. 85 (2022) 056201, https://doi.org/10.1088/1361-6633/ac5754.

[4] Y. Meng et al, Dark Matter Search Results from the PandaX-4T Commissioning Run, Phys. Rev. Lett. 127 (2021) 261802, https://doi.org/10.1103/PhysRevLett.127.261802.

[5] E. Aprile et al (XENON Collaboration), Search for New Physics in Electronic Recoil Data from XENONnT, Phys. Rev. Lett. 129 (2022) 161805, https://doi.org/10.1103/PhysRevLett.129.161805.

[6] J. Aalbers (LZ Collaboration), First Dark Matter Search Results from the LUX-ZEPLIN (LZ) Experiment, arXiv:2207.03764, https://doi.org/10.48550/arXiv.2207.03764.

[7] R. Ajaj et al (DEAP Collaboration), Search for dark matter with a 231-day exposure of liquid argon using DEAP-3600 at SNOLAB, Phys. Rev. D 100 (2019) 022004, https://doi.org/10.1103/PhysRevD.100.022004.

[8] P. Agnes et al (The DarkSide Collaboration), DarkSide-50 532-day dark matter search with low-radioactivity argon, Phys. Rev. D 98 (2018) 102006, https://doi.org/10.1103/PhysRevD.98.102006.

[9] P. Agnes et al (The DarkSide Collaboration), Low-Mass Dark Matter Search with the DarkSide-50 Experiment, Phys. Rev. Lett. 121 (2018) 08130, https://doi.org/10.1103/PhysRevLett.121.081307; Search for low-mass dark matter WIMPs with 12 ton-day exposure of DarkSide-50, arXiv:2207.11966, https://doi.org/10.48550/arXiv.2207.11966; Search for dark matter-nucleon interactions via Migdal eleectron with DarkSide-50, arXiv:2207.11967, https://doi.org/10.48550/arXiv.2207.11967.

[10] P. Agnes et al (The DarkSide Collaboration), Constraints on Sub-GeV Dark-Matter Electron Scattering from the DarkSide-50 Experiment, Phys. Rev. Lett. 121 (2018) 111303, https://doi.org/10.1103/PhysRevLett.121.111303; Search for dark matter particle interactions with electron final states with DarkSide-50, arXiv:2207.11968, https://doi.org/10.48550/arXiv.2207.11968.

[11] G. Heusser, Low-radioactivity background techniques, Annu. Rev. Nucl. Part. Sci. 45 (1995) 543, https://doi.org/10.1146/annurev.ns.45.120195.002551.

[12] J.A. Formaggio and C.J. Martoff, Backgrounds to sensitive experiments underground, Annu. Rev. Nucl. Part. Sci. 54 (2004) 361, https://doi.org/10.1146/annurev.nucl.54.070103.181248.

[13] S. Cebrián, Cosmogenic activation of materials, Int. J. Mod. Phys. A 32 (2017) 1743006, https://doi.org/10.1142/S0217751X17430060.

[14] S. Cebrián, Cosmogenic Activation in Double Beta Decay Experiments, Universe 6 (2020) 162, https://doi.org/10.3390/universe6100162.

[15] I. Barabanov et al, Cosmogenic activation of germanium and its reduction for low background experiments, Nucl. Instrum. Meth. B 251 (2006) 115–120, https://doi.org/10.1016/j.nimb.2006.05.011.

[16] D. M. Mei et al, Cosmogenic production as a background in searching for Rare Physics processes, Astropart. Phys. 31 (2009) 417–420, https://doi.org/10.1016/j.astropartphys.2009.04.004.

[17] S. R. Elliott et al, Fast-neutron activation of long-lived isotopes in enriched Ge, Phys. Rev. C 82 (2010) 054610, https://doi.org/10.1103/PhysRevC.82.054610.

[18] S. Cebrián et al, Cosmogenic activation in germanium and copper for rare event searches, Astropart. Phys. 33 (2010) 316–329, https://doi.org/10.1016/j.astropartphys.2010.03.002.

[19] E. Armengaud et al, Measurement of the cosmogenic activation of germanium detectors in EDELWEISS-III, Astropart. Phys. 91 (2017) 51–64, https://doi.org/10.1016/j.astropartphys.2017.03.006.

[20] J. Amaré et al, Cosmogenic production of tritium in dark matter detectors, Astropart. Phys. 97 (2018) 95–105, https://doi.org/10.1016/j.astropartphys.2017.11.004.

[21] R. Agnese et al, Production Rate Measurement of Tritium and Other Cosmogenic Isotopes in Germanium with CDMSlite, Astropart. Phys. 104 (2019) 1-12, https://doi.org/10.1016/j.astropartphys.2018.08.006.

[22] J. L. Ma et al, Study on cosmogenic activation in germanium detectors for future tonne-scale CDEX experiment, Science China-Physics, Mechanics and Astronomy 62 (2019) 011011, https://doi.org/10.1007/s11433-018-9215-0.

[23] Y.L. Yan et al, Study on cosmogenic radioactive production in germanium as a background for future rare event search experiments, Nucl. Sci. Tech. 31 (2020) 55, https://doi.org/10.1007/s41365-020-00762-1.

[24] R. Saldanha et al, Cosmogenic activation of silicon, Phys. Rev. D 102 (2020) 102006, https://doi.org/10.1103/PhysRevD.102.102006.

[25] J. Amaré et al, Cosmogenic radionuclide production in NaI(Tl) crystals, J. Cosm. Astrop. Phys. 02 (2015) 046, https://doi.org/10.1088/1475-7516/2015/02/046.

[26] P. Villar et al, Study of the cosmogenic activation in NaI(Tl) crystals within the ANAIS experiment, Int. J. Mod. Phys. A 33 (2018) 1843006, https://doi.org/10.1142/S0217751X18430066.

[27] E. Barbosa de Souza et al, Study of cosmogenic radionuclides in the COSINE-100 NaI(Tl) detectors, Astropart. Phys. 115 (2020) 102390, https://doi.org/10.1016/j.astropartphys.2019.102390.

[28] R. Saldanha et al, Cosmogenic activation of sodium iodide, Phys. Rev. D 107 (2023) 022006, https://doi.org/10.1103/PhysRevD.107.022006.

[29] A. F. Barghouty et al, Measurements of p-induced radionuclide production cross sections to evaluate cosmic-ray activation of Te, Nucl. Instrum. Meth. B 295 (2013) 16–21, https://doi.org/10.1016/j.nimb.2012.10.008.

[30] V. Lozza and J. Petzoldt, Cosmogenic activation of a natural tellurium target, Astropart. Phys. 61 (2015) 62–71, https://doi.org/10.1016/j.astropartphys.2014.06.008.

[31] B.S. Wang et al, Cosmogenic-neutron activation of TeO_2 and implications for neutrinoless double-beta decay experiments, Phys. Rev. C 92 (2015) 024620, https://doi.org/10.1103/PhysRevC.92.024620.

[32] L. Baudis et al, Cosmogenic activation of xenon and copper, Eur. Phys. J. C 75 (2015) 485, https://doi.org/10.1140/epjc/s10052-015-3711-3.

[33] C. Zhang et al, Cosmogenic activation of materials used in rare event search experiments, Astropart. Phys. 84 (2016) 62–69, https://doi.org/10.1016/j.astropartphys.2016.08.008.

[34] J. Aalbers et al, Cosmogenic production of ^{37}Ar in the context of the LUX-ZEPLIN experiment, Phys. Rev. D 105 (2022) 082004, https://doi.org/10.1103/PhysRevD.105.082004.

[35] R. Saldanha et al, Cosmogenic production of ^{39}Ar and ^{37}Ar in argon, Phys. Rev. C 100 (2019) 024608, https://doi.org/10.1103/PhysRevC.100.024608.

[36] C. Zhang and D.M. Mei, Evaluation of cosmogenic production of ^{39}Ar and ^{42}Ar for rare-event physics using underground argon, Astropart. Phys. 142 (2022) 102733, https://doi.org/10.1016/j.astropartphys.2022.102733.

[37] W. Chen et al, Cosmogenic background study for a ^{100}Mo-based bolometric demonstration experiment at China Jin-Ping underground Laboratory, Eur. Phys. J. C 82 (2022) 549, https://doi.org/10.1140/epjc/s10052-022-10501-y.

[38] M. Laubenstein, G. Heusser, Cosmogenic radionuclides in metals as indicator for sea level exposure history, App. Rad. Isot. 67 (2009) 750–754, https://doi.org/10.1016/j.apradiso.2009.01.029.

[39] Z. She et al, Study on cosmogenic activation in copper for rare event search experiments, Eur. Phys. J. C 81 (2021) 1041, https://doi.org/10.1140/epjc/s10052-021-09827-w.

[40] V.E. Guiseppe et al, Fast-neutron activation of long-lived nuclides in natural Pb, Astropart. Phys. 64 (2015) 34–39, https://doi.org/10.1016/j.astropartphys.2014.11.002.

[41] C. A. J. O'Hare, New Definition of the Neutrino Floor for Direct Dark Matter Searches, Phys. Rev. Lett. 127 (2021) 251802, https://doi.org/10.1103/PhysRevLett.127.251802.

[42] A. Gaspert et al, Neutrino backgrounds in future liquid noble element dark matter direct detection experiments, Phys. Rev. D 105 (2022) 035020, https://doi.org/10.1103/PhysRevD.105.035020.

[43] P. Agnes et al, Sensitivity of future liquid argon dark matter search experiments to core-collapse supernova neutrinos, JCAP 03 (2021) 043, https://doi.org/10.1088/1475-7516/2021/03/043.

[44] P. Agnes et al, Separating ^{39}Ar from ^{40}Ar by cryogenic distillation with Aria for dark-matter searches, Eur. Phys. J. C 81 (2021) 359, https://doi.org/10.1140/epjc/s10052-021-09121-9.

[45] C.E. Aalseth et al (The DarkSide-20k collaboration), Design and construction of a new detector to measure ultra-low radioactive-isotope contamination of argon, JINST 15 (2020) P02024, https://doi.org/10.1088/1748-0221/15/02/P02024.

[46] E. Church, Ch. Jackson, R. Saldanha, Dark Matter Detection Capabilities of a Large Multipurpose Liquid Argon Time Projection Chamber, JINST 15 (2020) P092026, https://doi.org/10.1088/1748-0221/15/09/P09026.

[47] T. Alexander et al, The Low-Radioactivity Underground Argon Workshop: A workshop synopsis, arXiv:1901.10108, https://doi.org/10.48550/arXiv.1901.10108.

[48] H. O. Back et al, A Facility for Low-Radioactivity Underground Argon, Snowmass2021 white Paper, arXiv:2203.09734, https://doi.org/10.48550/arXiv.2203.09734.

[49] P. Agnes et al, Sensitivity projections for a dual-phase argon TPC optimized for light dark matter searches through the ionization channel, arXiv:2209.01177, https://doi.org/10.48550/arXiv.2209.01177.

[50] P. Adhikari et al (DEAP Collaboration), First Direct Detection Constraints on Planck-Scale Mass Dark Matter with Multiple-Scatter Signatures Using the DEAP-3600 Detector, Phys. Rev. Lett. 128 (2022) 011801, https://doi.org/10.1103/PhysRevLett.128.011801.

[51] P. Agnes et al, Simulation of argon response and light detection in the DarkSide-50 dual phase TPC, JINST 12 (2017) P10015, https://doi.org/10.1088/1748-0221/12/10/P10015.

[52] M. S. Gordon et al, Measurement of the Flux and Energy Spectrum of Cosmic-Ray Induced Neutrons on the Ground, IEEE Trans. Nucl. Sci. 51 (2004) 3427–3434, https://doi.org/10.1109/TNS.2004.839134. Erratum: M. S. Gordon et al, IEEE Transactions on Nuclear Science 52 (2005) 2703.

[53] J.F. Ziegler, Terrestrial cosmic ray intensities, IBM J. Res. Dev. 42 (1998) 117, https://doi.org/10.1147/rd.421.0117.

[54] N. Otuka et al, Towards a More Complete and Accurate Experimental Nuclear Reaction Data Library (EXFOR): International Collaboration Between Nuclear Reaction Data Centres (NRDC), Nucl. Data Sheets 120 (2014) 272, https://doi.org/10.1016/j.nds.2014.07.065.

[55] R. Silberberg and C. H. Tsao, Partial Cross-Sections in High-Energy Nuclear Reactions, and Astrophysical Applications. I. Targets With z<=28, Astrophys. J. Suppl. Ser. 25 (1973) 315; ibid p. 335.

[56] R. Silberberg and C. H. Tsao, Cross sections for (p, xn) reactions, and astrophysical applications, Astrophys. J. Suppl. Ser. 35 (1977) 129; Improved cross section calculations for astrophysical applications, Astrophys. J. Suppl. Ser. 58 (1985) 873; Spallation processes and nuclear interaction products of cosmic rays, Phys. Rep. 191 (1990) 351.

[57] R. Silberberg and C. H. Tsao, Updated partial cross sections of proton-nucleus reactions, Astrophys. J. 501 (1998) 911, https://doi.org/10.1086/305862.

[58] J. Martoff and P.D. Lewin, COSMO- a program to estimate spallation radioactivity produced in a pure substance by exposure to cosmic-radiation on the Earth, Comput. Phys. Commun. 72 (1992) 96, https://doi.org/10.1016/0010-4655(92)90008-M.

[59] J.J. Back, Y.A. Ramachers, ACTIVIA: Calculation of isotope production cross-sections and yields, Nucl. Instrum. Meth. A 586 (2008) 286-294, https://doi.org/10.1016/j.nima.2007.12.008.

[60] J.C. David, Spallation reactions: A successful interplay between modeling and applications, Eur. Phys. J. A 51 (2015) 68, https://doi.org/10.1140/epja/i2015-15068-1.

[61] J. Allison et al, Recent developments in Geant4, Nucl. Instrum. Meth. A 835 (2016) 186, https://doi.org/10.1016/j.nima.2016.06.125.

[62] T.T. Böhlen et al, The FLUKA Code: Developments and Challenges for High Energy and Medical Applications, Nuclear Data Sheets 120 (2014) 211, https://doi.org/10.1016/j.nds.2014.07.049.

[63] A. J. Koning et al, TENDL: Complete Nuclear Data Library for Innovative Nuclear Science and Technology, Nucl. Data Sheets 155 (2019) 1, https://doi.org/10.1016/j.nds.2019.01.002.

[64] K. Shibata et al, JENDL-4.0: A New Library for Nuclear Science and Engineering, J. Nucl. Sci. Technol. 48 (2011) 1, https://doi.org/10.1080/18811248.2011.9711805.

[65] Y. A. Korovin et al, High Energy Activation Data Library (HEAD-2009), Nucl. Instrum. Meth. A 624 (2010) 20–26, https://doi.org/10.1016/j.nima.2010.08.110.

[66] Decay Data Evaluation Project, http://www.nucleide.org/DDEP.htm.

[67] D.S. Akerib et al, Radio-assay of Titanium samples for the LUX Experiment, arXiv:1112.1376, https://arxiv.org/abs/1112.1376.

[68] D.S. Akerib et al, Identification of radiopure titanium for the LZ dark matter experiment and future rare event searches, Astropart. Phys. 96 (2017) 1, https://doi.org/10.1016/j.astropartphys.2017.09.002.

[69] E. Aprile et al, Material radioassay and selection for the XENON1T dark matter experiment, Eur. Phys. J. 77 (2017) 890, http://dx.doi.org/10.1140/epjc/s10052-017-5329-0.

[70] The Lundl/LBNL Nuclear Data Search, http://nucleardata.nuclear.lu.se/toi.

[71] P. Benetti et al, Measurement of the specific activity of ^{39}Ar in natural argon, Nucl. Instrum. Meth. A 574 (2007) 83, https://doi.org/10.1016/j.nima.2007.01.106.

[72] J. Calvo et al, Backgrounds and pulse shape discrimination in the ArDM liquid argon TPC, JCAP 12 (2018) 011, https://doi.org/10.1088/1475-7516/2018/12/011.

[73] R. Ajaj et al (DEAP Collaboration), Electromagnetic Backgrounds and Potassium-42 Activity in the DEAP-3600 Dark Matter Detector, Phys. Rev. D 100 (2019) 072009, https://doi.org/10.1103/PhysRevD.100.072009.

[74] P. Agnes et al (DarkSide Collaboration), Results from the first use of low radioactivity argon in a dark matter search, Phys. Rev. D 93 (2016) 081101(R), https://doi.org/10.1103/PhysRevD.93.081101.

[75] A. Lubashevskiy et al, Mitigation of ^{42}Ar/^{42}K background for the GERDA Phase II experiment, Eur. Phys. J. C 78 (2018) 15, https://doi.org/10.1140/epjc/s10052-017-5499-9.

[76] A.J. Peurrung et al, Expected atmospheric concentration of ^{42}Ar, Nucl. Instrum. Meth. A 396 (1997) 524, https://doi.org/10.1016/S0168-9002(97)00819-X.

[77] P. Cennini et al, On atmospheric ^{39}Ar and ^{42}Ar abundance, Nucl. Inst. Meth. A 356 (1995) 526, https://doi.org/10.1016/0168-9002(94)01234-2.

[78] A.S. Barabash, R.R. Saakyan, V.I. Umatov, On concentration of ^{42}Ar in liquid argon, J. Phys.: Conf. Ser. 718 (2016) 062004, https://doi.org/10.1088/1742-6596/718/6/062004.

[79] J. Amaré et al, Cosmogenic production of tritium in dark matter detectors, Astropart. Phys. 97 (2018) 96, https://doi.org/10.1016/j.astropartphys.2017.11.004.

[80] J. Amaré et al, Analysis of backgrounds for the ANAIS-112 dark matter experiment, Eur. Phys. J. C 79 (2019) 412, https://doi.org/10.1140/epjc/s10052-019-6911-4.

[81] P. Adhikari et al, Background model for the NaI(Tl) crystals in COSINE-100, Eur. Phys. J. C 78 (2018) 490, https://doi.org/10.1140/epjc/s10052-018-5970-2.

[82] E. Aprile et al (XENON Collaboration), Observation of Excess Electronic Recoil Events in XENON1T, Phys. Rev. D 102 (2020) 072004, https://doi.org/10.1103/PhysRevD.102.072004.

[83] A.E. Robinson, XENON1T observes tritium, arXiv:2006.13278, https://doi.org/10.48550/arXiv.2006.13278.

[84] D. H. Meikrantz et al, Tritium Process Applications Using SAES Getters for Purification and Collection from Inert Gas Streams, Fus. Technol. 27 (1995) 14, https://doi.org/10.13182/FST95-A11963799.

[85] S. MacMullin et al, Partial γ-ray production cross sections for (n,xnγ) reactions in natural argon at 1-30 MeV, Phys. Rev. C 85 (2012) 064614, https://doi.org/10.1103/PhysRevC.85.064614.

[86] S. M. Qaim, R. Wolfle, Triton emission in the interactions of fast neutrons with nuclei, Nucl. Phys. A 295 (1978) 150–162, https://doi.org/10.1016/0375-9474(78)90026-X.